Behavior of the Three-Phase Induction Motor With Spiral Sheet Rotor

Ramon Mujal Rosas, Oriol Boix Aragonès, *Senior Member, IEEE*, Xavier Colom Fajula, and Alejandro Rolán Blanco

***Abstract*—Improvements in torque at low currents using a rotor with spiral sheets are analyzed. Several rotors and stators have been built combining different constructive and mechanical characteristics of the related elements: inertias, constructive materials, geometrical shapes of the sheets, and geometrical disposition of the sheets. These different types of motors have been simulated using computer-aided tools and then tested in the laboratory. Finally, four stators (1000, 1500, 1500-type A, and 3000 r/min), with the same constructive parameters, have been simulated and tested with the following rotors types: solid rotor, solid rotor with diamagnetic rings, drag cup, and simple and double squirrel cage rotor; the results have been compared to those obtained with the seven variants of the spiral sheet rotor presented in this paper.**

***Index Terms*—Electric machines, special machine, spiral sheet rotor, three-phase asynchronous motor.**

I. Introduction

THE ROTORS of conventional asynchronous motors are formed by magnetic sheets packed above the shaft of the machine. The rotating magnetic field created by the stator induces currents parallel to the shaft and thus upright to the rotor sheets [1]. These currents cannot flow between the sheets if they are electrically isolated, requiring the intervention of conventional squirrel cage rings to close the electric circuit so that the rotor currents can circulate.

Typical configurations of three-phase asynchronous motors [2] are shown in Fig. 1 and described in the following points.

1) Single cage winding with high resistance and minimal inductance.
2) Deep slot cage, with low resistance and progressive reactance with the slip.
3) Low resistance and low reactance slot.
4) Finally, there are additional configurations of double and triple cage combining characteristics of the previous dispositions, with different resistance and reactance values for each cage.

In all of these dispositions, currents go through the cage conductors [3], while magnetic field goes through the sheets. The performance of these motors depends on the magnetic field, the current, and the distance from the conductor to the shaft.

Manuscript received December 4, 2007; revised February 6, 2008. First published January 20, 2009; current version published February 19, 2009. This work was supported by the "Ministerio de Ciencia y Tecnología de España" under DPI 2004-03180 Research Project. Paper no. TEC-00476-2007.

R. M. Rosas, O. B. Aragonès, and A. R. Blanco are with the Department of Electrical Engineering, Technical University of Catalonia, 08222 Terrassa, Spain (e-mail: mujal@ee.upc.edu; boix@ee.upc.edu; alejandro.rolan@upc.edu).

X. C. Fajula is with the Department of Chemical Engineering, Technical University of Catalonia, 08222 Terrassa, Spain (e-mail: xavier.colom@upc.edu).

Digital Object Identifier 10.1109/TEC.2008.2005283

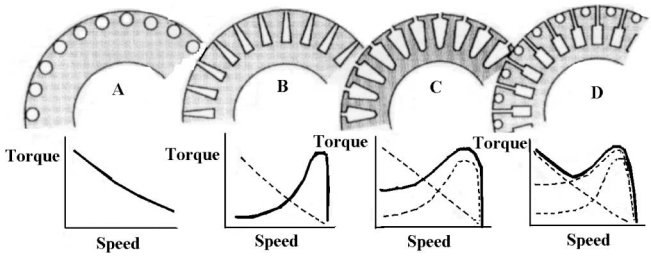

Fig. 1. Typical configurations of three-phase asynchronous motors.

TABLE I
MAIN MECHANICAL CHARACTERISTICS OF ROTORS

Rotor types	Mass (kg)	Inertia ($kg \cdot m^2$)	Kinetic energy at 1500 rpm (J)	Rotor dimensions (mm)
Squirrel cage	3.440	$2.717 \cdot 10^{-3}$	33.519	79.5 x 71
Solid rotor	3.620	$2.860 \cdot 10^{-3}$	35.283	79.5 x 71
Solid with ring	3.580	$2.828 \cdot 10^{-3}$	34.889	79.5 x 71
Diamagnetic hollow rotor	0.620	$4.898 \cdot 10^{-4}$	6.0426	79.5 x 71
Winding rotor	3.120	$2.465 \cdot 10^{-3}$	30.411	79.5 x 71
Spiral sheet, A	3.160	$2.496 \cdot 10^{-3}$	30.793	79.5 x 71
Spiral sheet, B	3.236	$2.556 \cdot 10^{-3}$	31.533	79.5 x 71
Spiral sheet, D	3.040	$2.401 \cdot 10^{-3}$	29.621	79.5 x 71
Spiral sheet, Z	3.230	$2.625 \cdot 10^{-3}$	32.384	79.5 x 71

II. Prototypes Description

As an example, the basic mechanical characteristics of some tested rotors are presented in Table I [3]. These rotors used have the same dimensions and are assembled to stators of 1000, 1500, and 3000 r/min, the latter having the same constructive parameters.

III. Three-Phase Asynchronous Torque Motor

The so-called torque-motor [5] is a three-phase asynchronous motor with the stator built in a classical way, but its rotor is constructed by a hard sheet iron cylinder (with small hysteresis cycle). With this kind of rotor, a higher useful section for flux circulation is obtained, but one of the drawbacks of this motor is the fact that the lines of magnetic fields go through its core reaching considerable depths, inducing an electromotive force (EMF) that makes it weaker.

A current circulating at greater depth has lower participation in the generation of torque, owing to the following causes.

1) Lower distance between the currents and the shaft of the motor.
2) The higher reactance results in lower power factor although the losses in the copper are the same as if they circulate on the periphery.

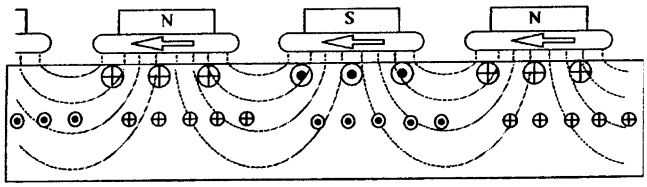

Fig. 2. Section of a "three-phase asynchronous torque-motor."

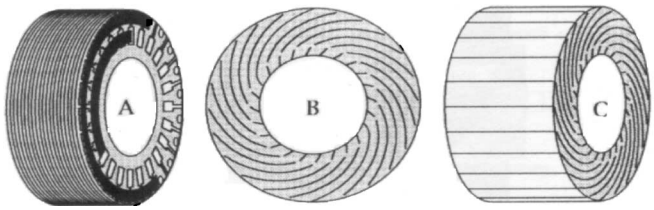

Fig. 3. Rotors: with double cage A. Spiral sheet rotors B and C types.

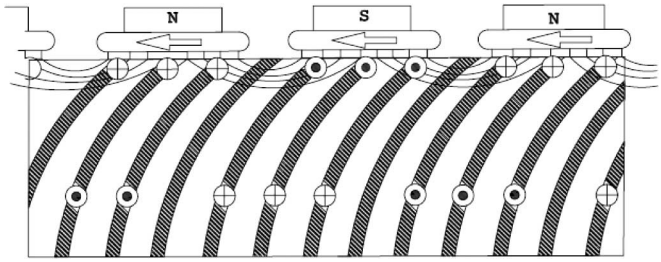

Fig. 4. Section of a "three-phase asynchronous torque-motor."

In Fig. 2, this phenomenon is illustrated showing that the deeper currents are weaker, and also have some delay in the direction of the displacement.

IV. Motor With a Spiral Sheet Rotor

Forming a rotor with spiral-shape sheets [8] distributed in a radial disposition around the shaft, it is possible to generate a magnetic field in the rotor periphery, inducing peripheral EMF, and currents along the same sheets, which are only active in their periphery.

The peripheral currents of this rotor have more section to circulate, compared to a normal cage rotor current, as can be seen in Fig. 3.

Fig. 4 shows a plain representation of the disposition of the sheets [9]. There are two zones: one with active currents going through and the other is used to receive the possible returning currents (a returning currents proposal).

The returning currents can be established in two ways, as shown in Fig. 5.

A) In the construction through short-circuit rings, the resistance corresponds to that of the outside of the iron sheets that form the rotor. This is because the short-circuit ring can be built in a big section, and its resistance can be despised compared to the resistance offered by the superficial sheets layers. This solution is not suitable for manufacturing; however, it gives the best results.

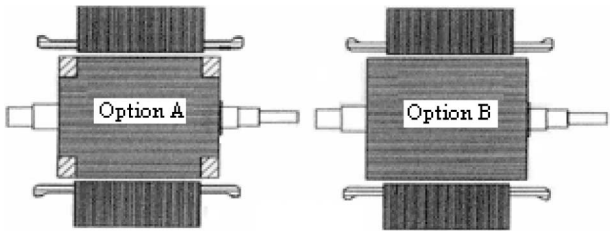

Fig. 5. (A) With short-circuit rings. (B) Without short-circuit rings.

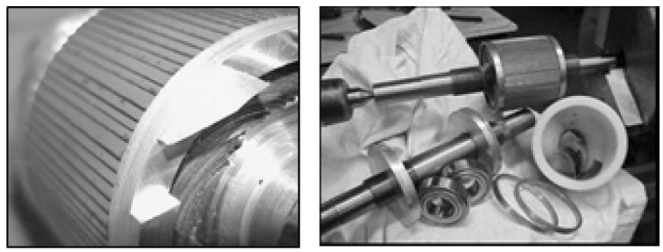

(a) (b)

Fig. 6. Rotor with spiral sheet in manufacturing phase. (a) Type A. (b) Type Z.

B) Part of the same sheet is a pathway for back currents that do not generate torque. In this case, the zones of active currents that generate torque are placed in the sheet periphery, and are affected by the magnetic field, leaving high sheet section as a return way.

V. Prototype Description

Several types of rotor have been constructed; each one is formed by a group of magnetic sheets radially disposed with the head directly above the shaft. These sheets completely cover the outside cylindrical surface of the shaft [8].

When sheet density is constant, in order to eliminate free space that would result in increasing the radial distance, the sheets have been rolled above the others as if the rotors were formed by a group of spinning sheets, as can be seen in Fig. 6.

In this way, the generated flux in the stator windings, which is the rotating magnetic field, falls in an inclined way into the sheets, producing some eddy currents that circulate in presence of the mentioned flux, generating some antagonistic torques. The outside torque is bigger than the inside one, because the radial distance is much higher, which results in a net rotation corresponding to the difference between the mentioned torques (see Fig. 7).

VI. Construction

To construct the proposed prototype rotor, a radically different process from the construction of a conventional squirrel cage rotor is followed.

It has been indicated that in this new rotor, the sheets do not have any slots. So, to have them perfectly joined without air spaces between them, its shape must have a perfect definite profile. This profile is reached by shaping with a tool or a matrix to deform every piece or sheet, giving the precise shape that is described as follows.

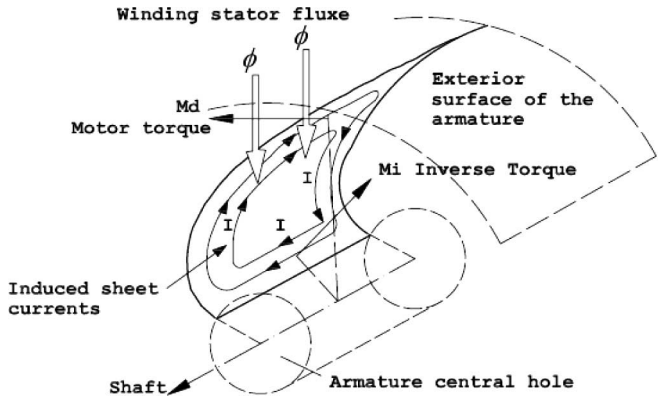

Fig. 7. Rotating magnetic field, eddy currents, and antagonistic torques.

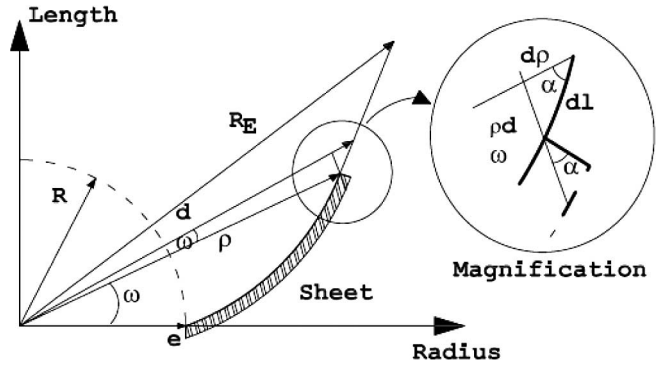

Fig. 8. Trigonometric relations of the sheet rotor.

If a rotor of interior radius R is considered, formed by n sheets of thickness e, where this thickness is very small compared to R, and with an outside radius R_E, then the trigonometric ratios shown in Fig. 8 are obtained.

A. Calculus of Length of the Sheet as a Function of the Interior Radius R and the Exterior Radius R_E

If the perimeter of the sheets is equal and grows with inside radius R and outside radius R_E, then

$$2\pi R = en \qquad 2\pi\rho = \frac{en}{\cos\,\alpha} \qquad \frac{R}{\rho} = \cos\,\alpha. \tag{1}$$

Also, from the differential triangle, knowing that both angles α are the same because of the perpendicular sides, then

$$dl = \frac{d\rho}{\cos\,\alpha} \qquad \text{or} \qquad dl = \frac{\rho d\rho}{R} \tag{2}$$

and by integrating

$$[L] = \left[\frac{\rho^2}{2R}\right]_R^{R_E} \qquad \text{and} \qquad L = \frac{\left(R_E^2 - R^2\right)}{2R}. \tag{3}$$

This is an expression that relates the length of every sheet with the interior radius R and the exterior one R_E, like the sheet illustrated in Fig. 9.

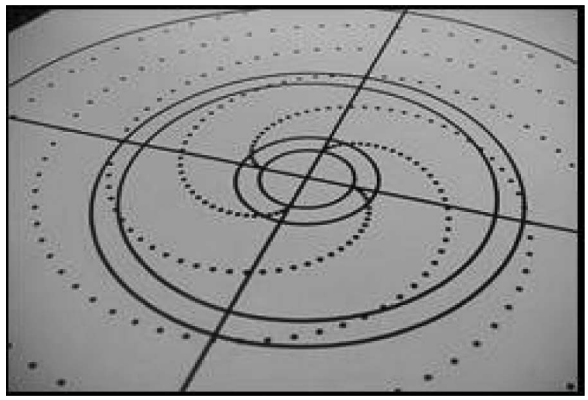

Fig. 9. Exact shape of the spiral sheets rotor.

B. Calculus of the Sheets Curvature Radius

Despite the knowledge of the relationship between the length and inside and outside radii, it is not enough to determine the exact shape that the sheets acquire. Another parameter, the sheet curvature radius, is necessary (sheets curve in every differential length). Starting from the known identities, the following equations hold:

$$\cos\,\alpha = \frac{R}{\rho} \qquad \text{and} \qquad \text{tg}\alpha = \frac{(\rho dw)}{d\rho} \tag{4}$$

$$\frac{d\rho}{dw} = \frac{\rho}{\text{tg}\alpha} = \frac{\rho\,(R/\rho)}{\sqrt{(1-\cos^2\,\alpha)}} = \frac{\rho R}{\sqrt{(R-\rho)}} = \rho'. \tag{5}$$

This is the differential polar equation that must be integrated between R_E and R limits to obtain, in every sheet's point, the required curve that accomplishes the objectives desired: perfect sheet junction without changing curve radius.

VII. Analysis of Conductivity

This section analyzes the distribution of currents versus the flux density of foil motors with different electric conductivity (3, 12, and 60 MS/m each one). The induction distribution and also the current density in the foils for 5-Hz rotor frequency are analyzed [7].

Fig. 10 shows that by increasing conductivity of the material, the current distribution becomes more superficial. From the analysis, we can appreciate the existence of a field created by the rotor as the conductivity of the material increases (see Fig. 11). According to the simulations, the net field in the motor is weaker as the rotor produces a bigger field. This phenomenon is only possible if there is a bigger phase between the two fields (stator and rotor). This space phase means a predictable change in the resistance and reactance properties in the rotor.

A bigger conductivity obviously implies a more inductive loading that generates a reactive power. The optimization in the selection of materials relapses in the evaluation of the product of the primary current by the factor of motor power with the useful torque that it can develop. This conclusion is very important because it is applicable to any part of the motor when deciding the application of the best materials.

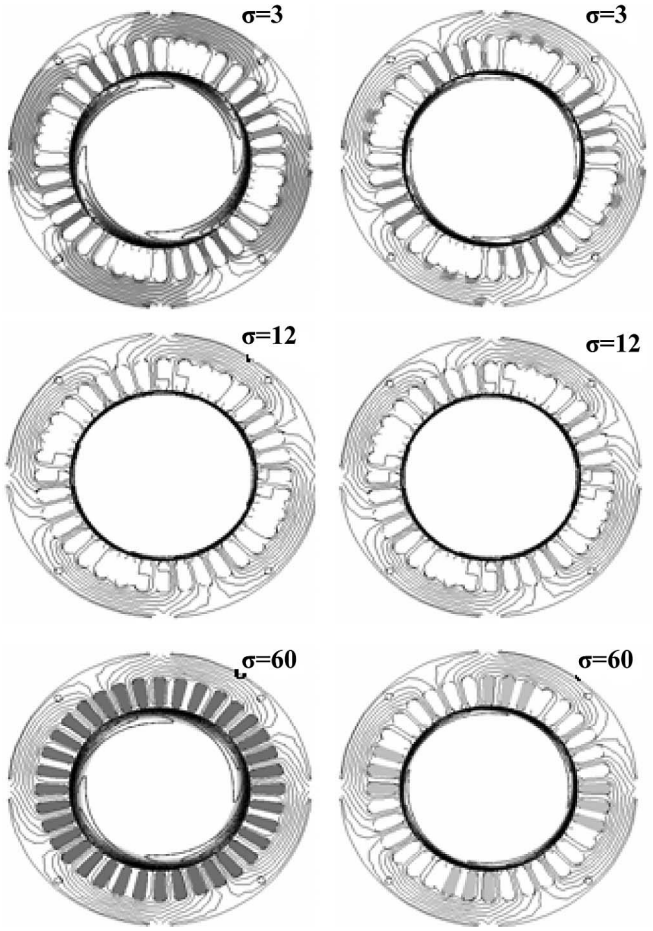

Fig. 10. Flux and current densities simulations for different conductivity values. The motor with spiral sheet rotor type A.

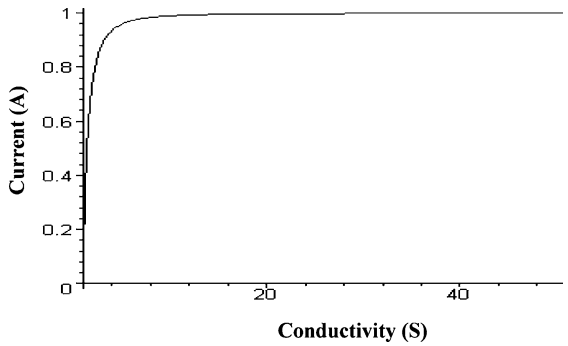

Fig. 11. Current conductivity in a motor with spiral sheet rotor.

Supposing the reactance variation in the rotor is very small, since its frequency is weak, it is possible to approach the variation of the angle of temporary phase out between the rotor current and the EMF as

$$\theta = \operatorname{arctg}(K\sigma) \tag{6}$$

where σ is the conductivity. Then, the width variation of B_{rotor} in relation to the I_{rotor} variation gives

$$\partial B \propto \partial I \qquad \text{and} \qquad I = \frac{\vec{E}}{R_{\text{rotor}} + jX_{\text{rotor}}} \tag{7}$$

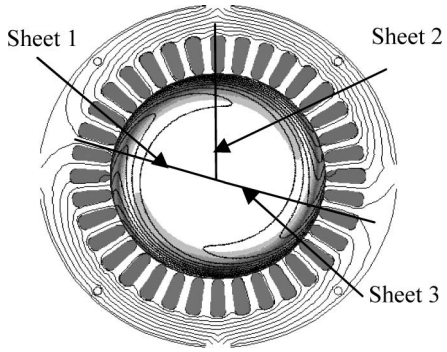

Fig. 12. Current density distribution.

with their corresponding module

$$\left|\vec{I}\right| = \frac{1}{R_{\text{rotor}}^2 + X_{\text{rotor}}^2}\left|\vec{E}\left(R_{\text{rotor}} - jX_{\text{rotor}}\right)\right| = \frac{E}{\sqrt{R_{\text{rotor}}^2 + X_{\text{rotor}}^2}}. \tag{8}$$

Finally, making a series development

$$|I| \propto \frac{1}{X_{\text{rotor}}} - \frac{1}{2X_{\text{rotor}}^3}R_{\text{rotor}}^2. \tag{9}$$

Graphically, the dependence of the current module with the conductivity for very small R_{rotor} gives

$$|I| = K_1 - \frac{K_2}{\sigma^2}. \tag{10}$$

The obstacles of air found in the rotor flow facilitate the creation of a characteristic reluctance of the motor. This phenomenon facilitates a very quick transient response. The high reluctance also comes accompanied by a low inertia that also supposes a low mechanical and electric time constant.

VIII. Current Density Distribution

Through finite-element method magnetics (FEMM) simulations (see Fig. 12), the distribution of current density in the rotor [6] can be determined. The real component of this current density is represented in Fig. 13.

It is important to see the evolution of current density with the radius, which is represented by a sine wave function as was expected. This current density versus the rotor radius follows a hyperbolic distribution, or more precisely, it follows a hyperbolic tangent. The values of some electric magnitudes can also be observed in these graphs. For example, the value of maximum current density in the rotor is approximately 1.6 A/mm^2.

IX. Thermal Values

Thermal experiments demonstrate that the motors present different characteristics with respect to conventional squirrel cage motors since the current, which is the main cause of the increase in stator winds temperature, practically does not change when changing the load [8], as shown in Figs. 14 and 15. This

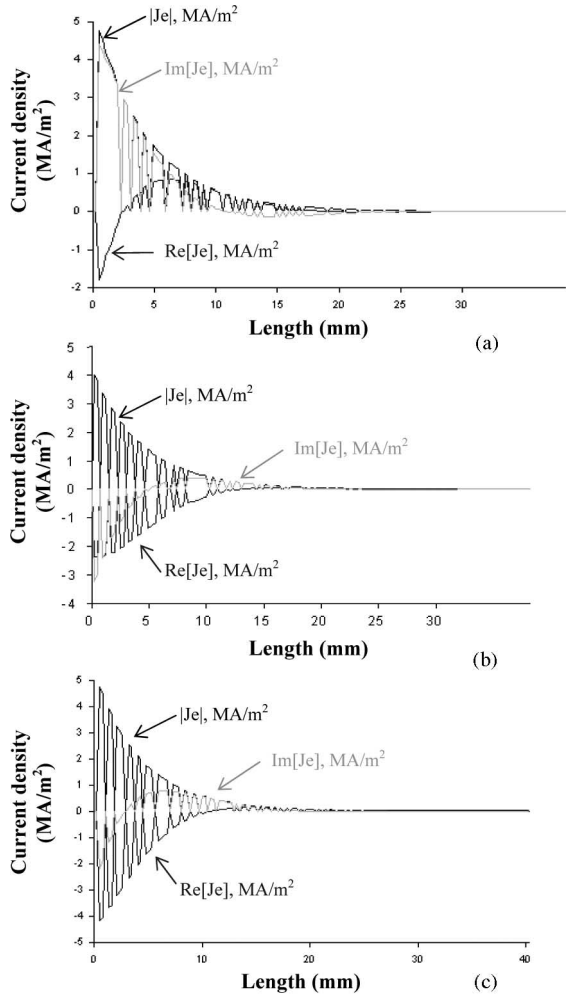

Fig. 13. Current density distribution. (a) Sheet 1. (b) Sheet 2. (c) Sheet 3.

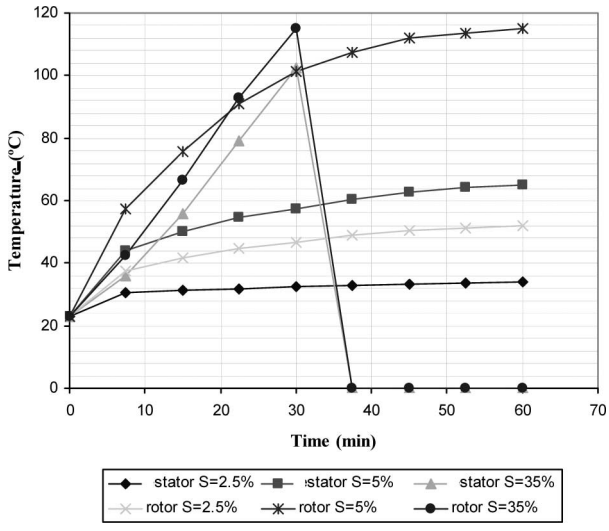

Fig. 14. Thermal test of the motor with squirrel cage rotor at 3000 r/min: evolution of rotor–stator temperature.

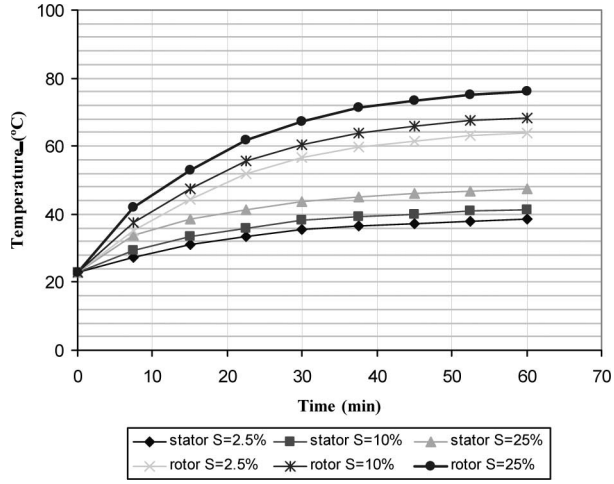

Fig. 15. Thermal test of the motor with spiral sheet rotor at 3000 r/min: evolution of rotor–stator temperature.

makes these motors able to work in regimes with high slip without changing their thermal conditions. This fact is almost impossible in squirrel cage motors.

On the other hand, the spiral sheet motors are more resistant than squirrel cage motors, and we can appreciate an increase of temperature with respect to squirrel cage rotors when they are working in the same conditions, but it is in any case much smaller than the increase that other rotors like the solid rotor undergo.

X. Electric Values

The following graphs (see Fig. 16) compare the behavior of a motor with a type A class spiral sheet rotor with a conventional squirrel cage motor, a motor with a solid rotor with rings, and a diamagnetic hollow rotor, all rotating at 3000 r/min.

It is observed that the motor with spiral sheet rotor shows better electrical behavior than the motor with a solid rotor, which is its closest competitor. In comparison with the squirrel cage motor, the motor with spiral sheet rotor has very favorable torque/current and torque/power ratios; thus, its performance is higher than the cage motor, with the exception of the last phase of the graph. Finally, torque is always lower than that obtained by the squirrel cage motor.

It could be understood that the advantages of the motor with spiral sheet rotor are given for unrated operating conditions (slip of 2%–3%). However, as verified by the thermal, mechanical, and magnetic analyses and unlike the squirrel cage motor, the motor with spiral sheet rotor can work continuously under higher slip values.

XI. Mechanical Inertias and Losses

The study of mechanical losses owing to the bearings, fan, and air friction has been made, getting reasonable values compared to the rest of conventional motors [1]. The inertias are very similar to squirrel cage motor values, and in the worst case, a light inertia increase in the spiral sheet motor is detected, which do not have a machined rotor, as can be seen in Figs. 17 and 18, in a stop–start cycle.

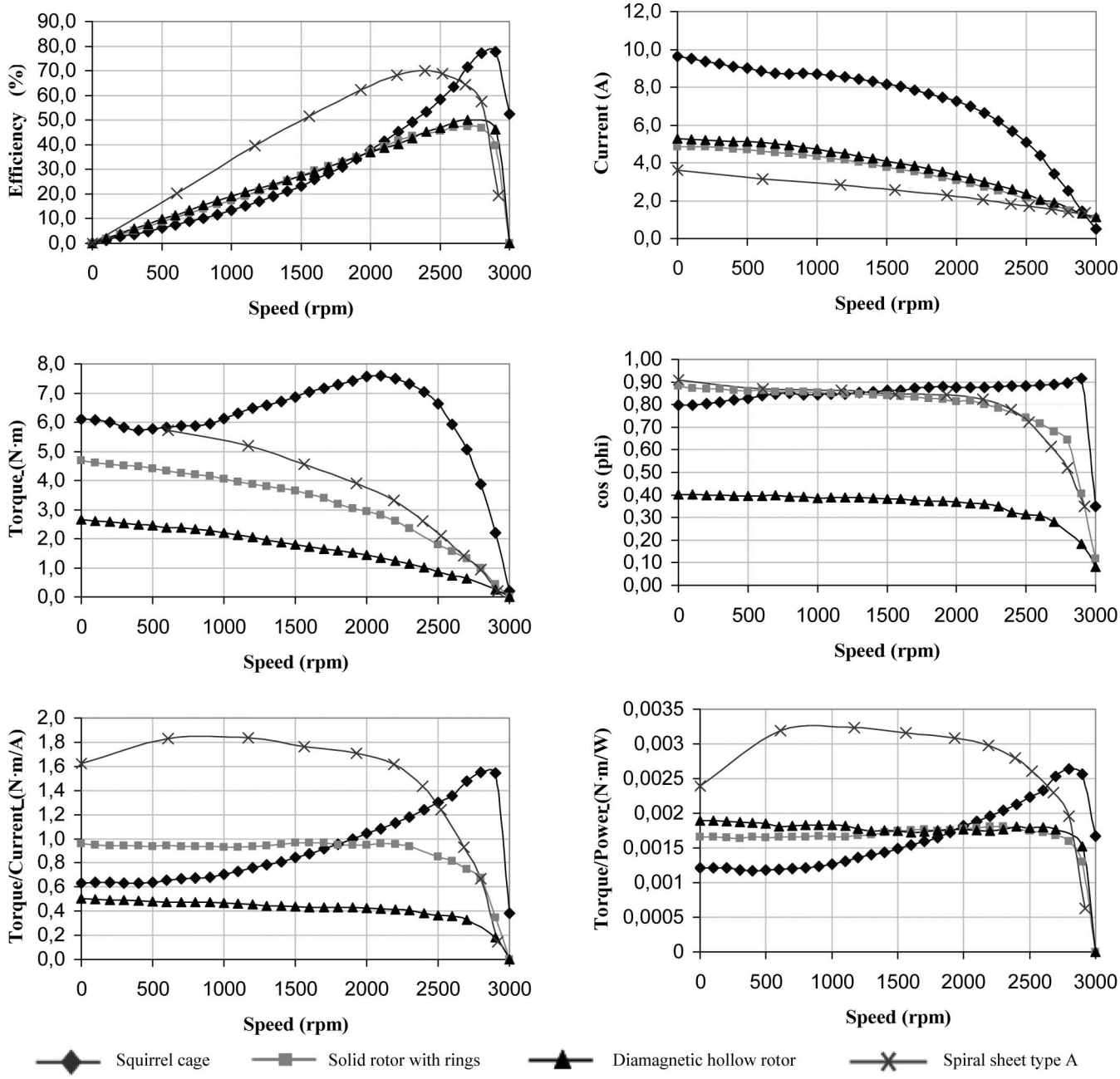

Fig. 16. Experimental results using different types of rotors (at 3000 r/min).

Finally, the experiments done to test mechanical resistance in long-term operation were satisfactory because although these rotors were not designed for periods of prolonged operations, they have not undergone any type of deformation.

XII. Parasitic Currents

Using simulation and a normal section test, it is possible to know the induction in a rotor (see Figs. 19 and 20).

With this distribution, the EMF results

$$E = -\frac{\partial \phi}{\partial t} = -\frac{\partial B}{\partial t} S = -SBw_S \cos\, w_S t \qquad (11)$$

where S is the magnetic circuit area, a constant in this case.

The current induced by this EMF in sheets can be calculated using the respective electric circuits, remembering that current flows inside the sheets. The EMF distribution is shown in Fig. 21.

This distribution is owing to the EMF in the upper area of the sheets inducing a higher current in this section (see Fig. 22). The maximum current can be calculated (r is the height of the sheets from the rotor axis center)

$$\left|\bar{E}_1\right| = \int_{R_{\text{axis}}}^{h} \frac{k}{(A-r)} dr = k \ln \frac{A - R_{\text{axis}}}{A-h} \qquad (12)$$

$$\left|\bar{E}_2\right| = \int_{h}^{R_{\text{stator}}} \frac{k}{(A-r)} dr = k \ln \frac{A-h}{A - R_{\text{stator}}} \qquad (13)$$

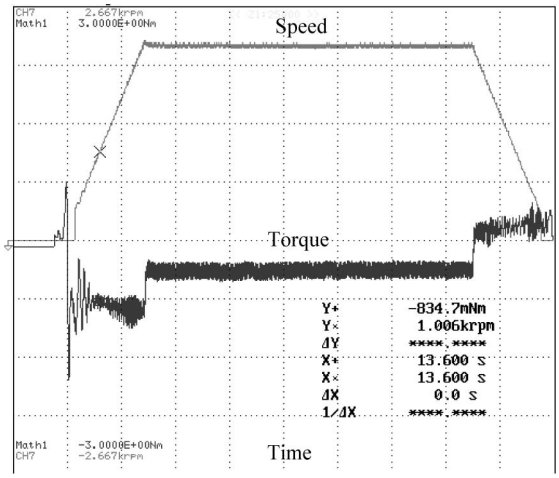

Fig. 17. Torque and speed in a stop–start cycle of a motor with squirrel cage rotor. Torque 0.75 N·m/div; speed 667 (r/min)/div; time 1s/div.

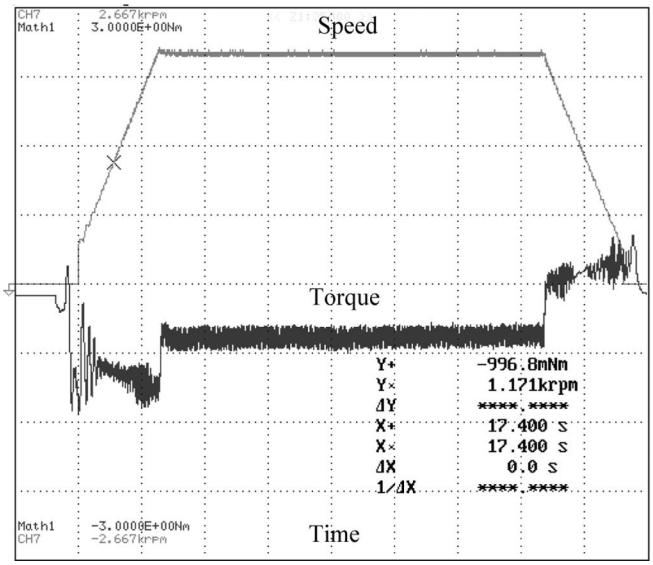

Fig. 18. Torque and speed in a stop–start cycle of a motor with spiral sheet rotor type A. Torque 0.75 N·m/div; speed 667 (r/min)/div; time 1s/div.

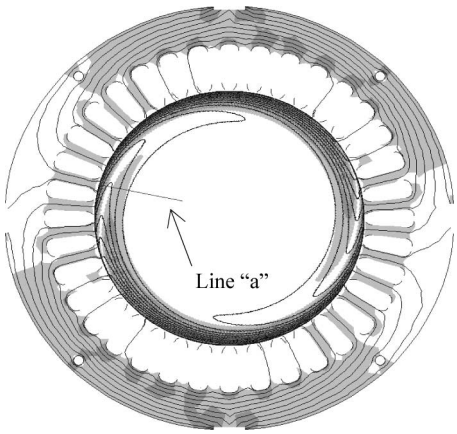

Fig. 19. Magnetic simulation with FEMM. Line "a" represents the section of simulation.

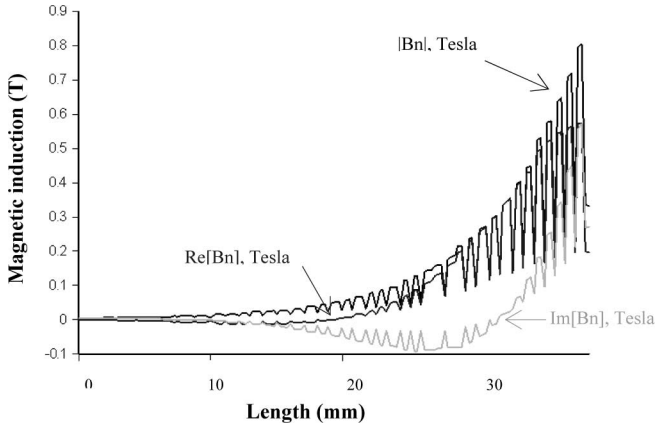

Fig. 20. Magnetic induction. Sheet rotor at 3000 r/min, $c = 3$ MS/m, $\mu = 4000$ H/m, and $f = 3.33$ Hz.

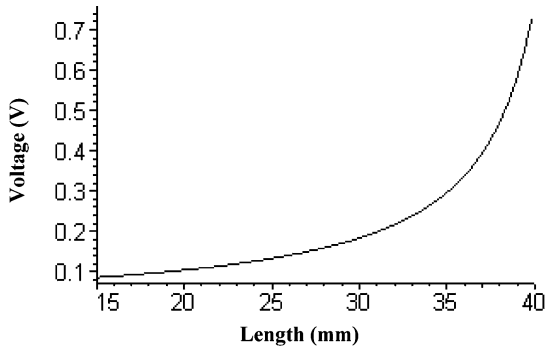

Fig. 21. EMF distribution (distance from stator axis).

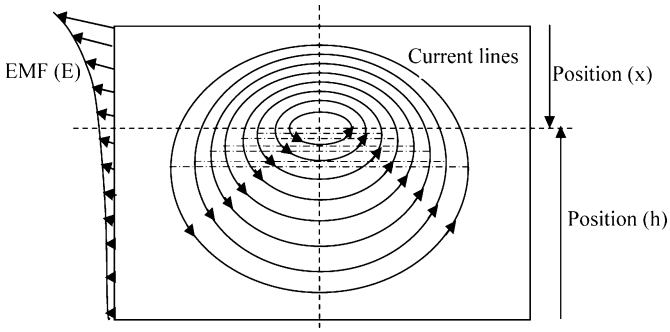

Fig. 22. Vertical coordinate defining the current sense change.

$$R_{\text{sheet}} = (R_1 + R_2) = \rho_{\text{sheet}} \frac{L_{\text{rotor}}}{e_{\text{sheet}}} \left(\frac{(R_{\text{stator}} - s)}{h(R_{\text{stator}} - h - s)} \right) \tag{14}$$

$$(E_1 - E_2) = I(R_1 + R_2) = k \ln \left[\frac{(A-h)^2}{(A - R_{\text{axis}})\,(A - R_{\text{stator}})} \right] \tag{15}$$

$$I = \frac{k \ln \left[(A-h)^2 / ((A - R_{\text{axis}})\,(A - R_{\text{stator}})) \right]}{\left[((\rho_{\text{sheet}} L_{\text{rotor}})/e_{\text{sheet}}) \right] \left[(R_{\text{stator}} - s)/(h(R_{\text{stator}} - h - s)) \right]} \tag{16}$$

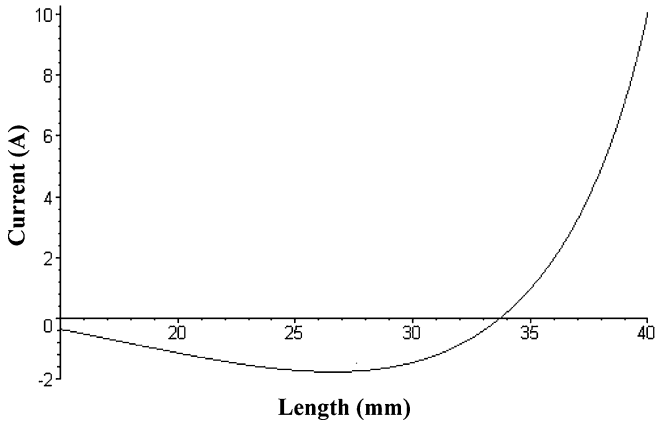

Fig. 23. Distribution of the active current along the radial sheet of the rotor.

where the constants A and k are values that adjust the electromagnetic field equation; s is a parameter that depends upon the current circulating through the upper sheet area; h is the sheet radius; $e_{\rm axis}$ is the sheet thickness (in millimeters); σ is the sheet conductivity (in siemens meter per square millimeter); $L_{\rm rotor}$ isthe rotor length.

As the induction is a function of the radial position of the considered section, which is known, it is possible to calculate the constants A and K

$$B_{\max} = \frac{K}{(A - R_{\rm stator})} \qquad A = \frac{B_{\min} R_{\rm rotor} - R_{\rm stator} B_{\max}}{B_{\min} - B_{\max}} \tag{17}$$

$$B_{\min} = \frac{K}{(A - R_{\rm rotor})} \qquad K = B_{\min}(A - R_{\rm rotor}) \tag{18}$$

and k is a constant function of maximum EMF

$$E = \frac{k}{(A - r)} \qquad k = E_{\max -2}(A - R_{\rm stator}) \tag{19}$$

$$E_{\max -2} = E_{\max -1} \left(\frac{m_1}{m_2}\right) \left(\frac{Z_2 \xi_2}{Z_1 \xi_1}\right) \tag{20}$$

where m_1 and m_2 are the number of phases of the stator and rotor; Z_1 and Z_2 are the number of turns and sheets of the stator and rotor; ξ_1 and ξ_2 are the distribution factors for the stator and rotor.

All the terms are known except the radial coordinate h that corresponds to a change of sense in the current along the shape profile.

With the coordinate h known, it is possible to calculate the total sheet current, by integration of the current equation between the upper and lower limits of the sheet (the distribution of the active current along the radial sheet is shown in Fig. 23)

$$I_{\rm upper} = \int_{h}^{R_{\rm stator}} \left[\left(\frac{k e_{\rm sheet}}{\rho_{\rm sheet} L_{\rm rotor}}\right) \ln\left[\frac{(A-h)^2}{(A-R_{\rm axis})\,(A-R_{\rm stator})}\right] \times \left[\frac{h(R_{\rm stator} - h - s)}{(R_{\rm stator} - s)}\right]\right] dh \tag{21}$$

$$I_{\rm lower} = \int_{R_{\rm rotor}}^{h} \left[\left(\frac{k e_{\rm sheet}}{\rho_{\rm sheet} L_{\rm rotor}}\right) \ln\left[\frac{(A-h)^2}{(A-R_{\rm axis})\,(A-R_{\rm stator})}\right] \times \left[\frac{h(R_{\rm stator} - h - s)}{(R_{\rm stator} - s)}\right]\right] dh \tag{22}$$

The ring per sheet current and the total currents are

$$I_{\rm ring\,per\,sheet} = I_{\rm upper} - I_{\rm lower} \tag{23}$$

$$I_{\rm total\,ring} = \frac{I_{\rm ring\,per\,sheet}}{2p} \times \frac{n_{\rm rotor\,sheets}}{\pi}. \tag{24}$$

The torque is related to this total current

$$\tau = \int_{R_{\rm rotor}}^{R_{\rm stator}} L_{\rm rotor} B(r) I(r) dh = L_{\rm rotor} \int_{R_{\rm rotor}}^{R_{\rm stator}} \left[\left(\frac{K}{(A-h)}\right)\left(\frac{k e_{\rm sheet}}{\rho_{\rm sheet} L_{\rm rotor}}\right) \times \ln\left[\frac{(A-h)^2}{(A-R_{\rm axis})\,(A-R_{\rm stator})}\right]\left(\frac{(h(R_{\rm stator}-h-s)}{(R_{\rm stator}-s)}\right)\right] dh. \tag{25}$$

XIII. Conclusion

The three-phase induction motor with spiral sheet rotor establishes several advantages in relation to conventional induction motors, namely, high starting torque with limited starting current, small current variations against load changes, moderated level of no-load power losses, acceptable efficiency in steady state, and good transient response.

The aforementioned performances make the proposed motor suitable for high-speed applications with frequent stops and starts, which means, in addition to a good electrical response, this motor should be characterized by good thermal behavior and high constructive robustness to withstand frequent speed variations.

A notable disadvantage is the high construction cost of the proposed motor compared to a conventional induction motor. This is mainly owing to the specialized tools used for mechanizing the sheets of the rotor and their sophisticated assembly. For this reason, this motor should be produced in large manufacturing lots.

Nowadays, a wide scope of applications exists requiring the aforementioned characteristics, notably, small staple fiber motors used in textile industries, drives for household appliances, machine tools, etc. Therefore, a widespread market could be expected for the proposed motor.

References

[1] X. Li, Q. Wu, and S. Nandi, "Performance analysis of a three-phase induction machine with inclined static eccentricity," *IEEE Trans. Ind. Appl.*, vol. 43, no. 2, pp. 531–541, Mar./Apr. 2007.

[2] D. Gonen, "Analysis of a 2-phase drag-cup induction machine," *IEEE Trans. Power App. Syst.*, vol. 85, no. 1, pp. 71–76, Jan. 1966.

[3] J. F. Lindsay and T. H. Barton, "Parameter identification for squirrel cage induction machines," *IEEE Trans. Power App. Syst.*, vol. 92, no. 1, pp. 1287–1291, Jan. 1996.

[4] R. Mujal and L. Humet, "Asynchronous motor with spiral sheet rotor," in *Proc. ICEM 2000*, Helsinki, Finland, Aug. 28–30, pp. 477–482.
[5] R. Mujal, "Asynchronous motor with spiral sheet rotor. Improvement of the functional characteristics of the asynchronous motors," in *Proc. ICEMS 2001*, Shenyang, China, Aug. 18–20, pp. 80–84.
[6] R. Mujal, "Three-phase asynchronous motor with spiral sheet rotor. Performance improvement of the three-phase induction motors," presented at the ISC 2002, Tsukuba, Japan, Aug. 26–28.
[7] R. Mujal, "Three-phase asynchronous motor with spiral sheet rotor. Material effects and analysis," in *Proc. IEEE Int. Electr. Mach. Drives Conf.,* Madison, USA, Mar. 1–4, 2003, pp. 1688–1694.
[8] R. Mujal, "Electromagnetic analysis of the induction motor with spiral sheet rotor," presented at the EPE 2005, Dresden, Germany, Sep. 12–15.
[9] R. Mujal, "Analysis of the induction motor with spiral sheet rotor," presented at the ICEM 2006, Crete, Greece, Sep. 4–6.
[10] R. Mujal and O. Boix, "Improvements of three phase induction motor with spiral sheet rotor," in *Proc. IEEE Int. Symp. Ind. Electron. ISIE 2007*, Vigo, Spain, Jun. 4–7, pp. 1107–1112.

Ramon Mujal Rosas was born in Cardona, Spain. He received the B.S. degree in electrical engineering and the Ph.D. degree in electrical engineering from the Technical University of Catalonia, Terrassa, Spain, in 1993 and 2004, respectively.

He is a currently a Professor in the Department of Electrical Engineering, Technical University of Catalonia. He is the author or coauthor of some books about electrical subjects, and is engaged in the areas of remote learning and special electrical machines.

Oriol Boix Aragonès (M'00–SM'06) was born in Barcelona, Spain. He received the B.S. degree in electrical engineering and the Ph.D. degree in electrical engineering from the Technical University of Catalonia, Terrassa, Spain, in 1988 and 1997, respectively.

He is a currently a Professor in the Department of Electrical Engineering, Technical University of Catalonia. His current research interests include Internet-based learning, harmonics, and power quality areas.

Xavier Colom Fajula was born in Sant Joan de les Abadesses, Spain. He received the B.S. degree in chemical engineering and the Ph.D. degree in material science from the Technical University of Catalonia, Terrassa, Spain, in 1991 and 1997, respectively.

He is a currently a Professor in the Department of Chemical Engineering, Technical University of Catalonia. He is the author or coauthor of several papers about polymer and composite materials, some books about material science subjects, and a referee of various journals.

Alejandro Rolán Blanco was born in Sabadell, Spain. He received the B.S. degree in electrical engineering in 2007 from the Technical University of Catalonia, Terrassa, Spain, where he is currently working toward the Doctorate degree in electrical engineering.

Since September 2007, he has been an Associate Professor in the Department of Electrical Engineering, Technical University of Catalonia.